Scratch Testing of Multilayered Metallic Film Stacks

Application Note

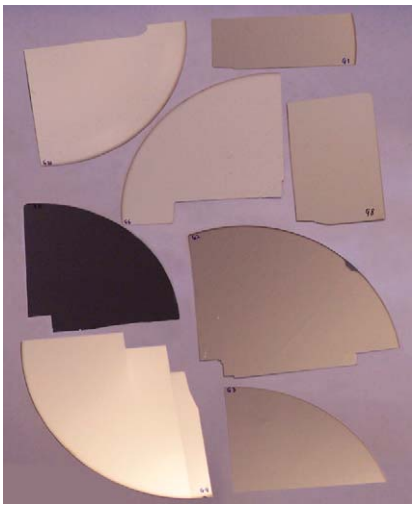

Figure 1. Wafer samples for testing.

Introduction

Historically, the mechanical performances of multilayered thin-film metal stacks have been difficult to characterize for failure by any means. Recent developments in nanoscratch techniques, though, have made great headway in the examination of film failure of these multilayered film stacks. Scratch testing has commonly been used for characterizing the adhesion of single films to the substrate materials. Now, with the ability to survey the surface before and after the scratch test, the scratch process can be used to evaluate the type of failure occurring at different interfaces throughout multilayered film stacks. In this study, eight film stacks were tested to examine failure in individual layers of the samples. All of the samples had between three and four metal layers ranging in thickness from 100 nm to 500 nm. These samples were labeled as "Good" or "Bad" by the manufacturer.

All of the samples were characterized using a ramp-load scratch test. The ramp-load scratch test was used for determination of the Critical Load for each layer in the film stack samples. Results from the scratch tests were used to define the difference in the scratch response between "Good" and "Bad" samples.

Samples

Eight film stack samples were supplied by a wafer manufacturer. The geometries of the samples are detailed in Table 1. Each sample consisted of three to four metal layers on a silicon substrate; the layers ranged in thickness from 100 nm to 500 nm. The wafer samples were diced and mounted to aluminum stubs for testing (Figure 1). For comparison purposes, the samples were divided into three groups based on the cross-sectional geometries and composition of the film layers (Table 1).

Group	Wafer No.	Wafer Description	Test Objective	Film Stack Thickness	Film Stack Composition
1	G1	Good	Measure critical load between metal stack and Si.	1100 nm	200 nm Al/200 nm Ti/ 500 nm NiV/200 nm Ag (Smooth)
	G4	Bad	Measure critical load between metal stack and Si. Oxide layer between Si and Al.		
	G9	Bad	Measure critical load between Ag and NiV. Oxide layer between NiV and Ag.		
2	G2	Good	Measure critical load between metal stack and Si.	500 nm	100 nm Ti/200 nm NiV/ 200 nm Ag (Smooth)
	G3	Bad	Measure critical load between metal stack and Si.		
	G6	Bad	Measure critical load between metal stack and Si.		
3	G8	Good	Measure critical load between metal stack and Si.	500 nm	100 nm Ti/200 nm NiV/ 200 nm Ag (Very Rough)
	G10	Bad	Measure critical load between Ag and NiV. Oxide layer between NiV and Ag.		

Table 1. Sample descriptions for the multilayered wafers and test objectives.

Agilent Technologies

Test Methodology

A ramp-load scratch test was used to conduct five tests on each sample. In a ramp-load scratch test, a tip is brought into contact with the sample; then, the tip is loaded at a constant loading rate while simultaneously translating the sample. Prior to and following the scratch cycle, a single-line scan of the surface topography is completed for comparison of the original surface to the deformation caused by the scratch cycle. Therefore, each scratch test consists of three steps: a single-line prescan of the area to be scratched, the ramp-load scratch cycle, and a final scan to evaluate the residual deformation. Before and after each step, a prescan and a postscan, usually equal to 20% of the scratch length, is performed so that the software can automatically align the data in the three steps. The original and residual single-line scans allow the evaluation of deformation mechanisms and the quantification of deformation. The scratch process is diagrammed in Figure 2. Test parameters that were used in the ramp-load scratch tests are listed in Table 2. The test loads varied depending on the sample that was being tested and the tip that was used for testing.

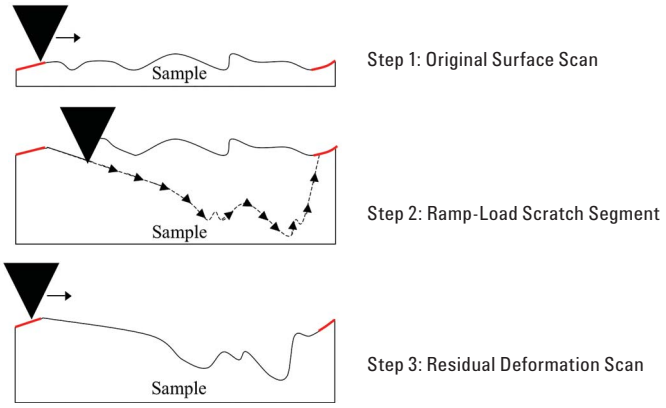

Figure 2. Diagram of the three-step ramp-load scratch test. Red lines show the areas of pre- and post-profile scans used to perform leveling of the three steps.

Group 1	Scratch Length	700 µm
	Scratch Velocity	30 µm/s
	Maximum Scratch Load	16 mN
	Scratch Tip and Orientation	Cube corner, face forward
Group 2	Scratch Length	700 µm
	Scratch Velocity	30 µm/s
	Maximum Scratch Load	25 mN
	Scratch Tip and Orientation	Cube corner, face forward
Group 3	Scratch Length	700 µm
	Scratch Velocity	30 µm/s
	Maximum Scratch Load	100 mN
	Scratch Tip and Orientation	90° cone, 1µm tip radius

Table 2. Test parameters for the ramp-load scratch tests.

Results and Discussion

GROUP 1

The samples in Group 1 consisted of four layers that totaled a thickness of 1100 nm. Ramp-load scratch testing was used to examine the failure of each layer as the test progressed. Figure 3 shows the load application as a function of scratch distance for the scratch tests performed on Group 1 samples.

Sample G1

Sample G1 did not exhibit unusual elastic deformation at the surface of the sample nor did it show blistering of any specific layer, but it did possess the highest Critical Load between the film stack and the Si substrate of all samples tested in Group 1. A graph of the displacement curves

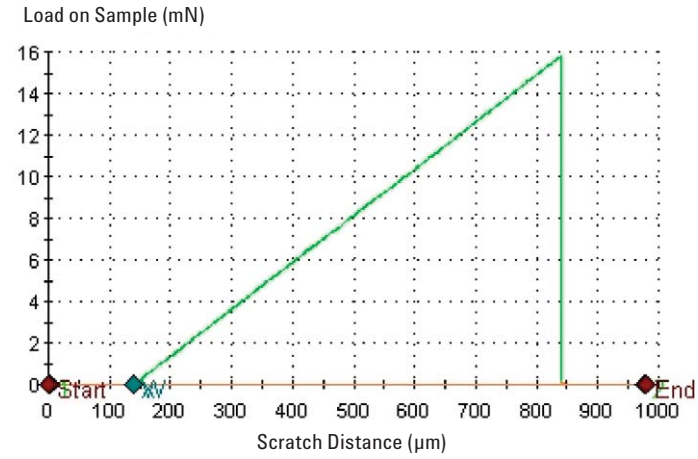

Figure 3. Load on sample versus scratch distance for the ramp-load scratch tests performed on the samples in Group 1.

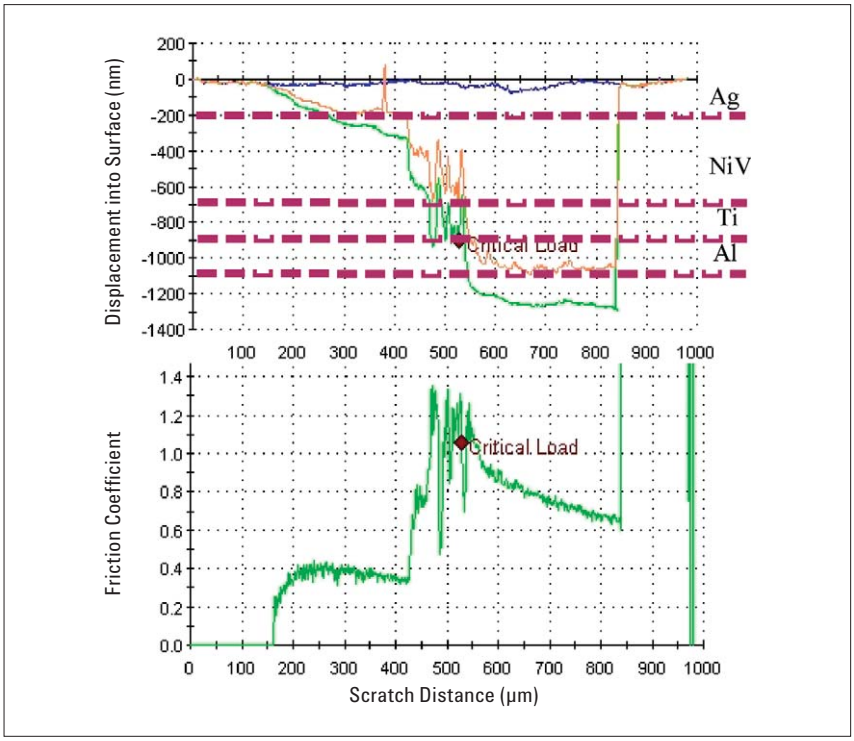

Figure 4. A plot of typical displacement curves and the coefficient of friction versus scratch distance for Sample G1. The original surface morphology (blue), Scratch cycle (green), and residual deformation (orange) are shown. The horizontal maroon lines indicate the locations of the film stack layers.

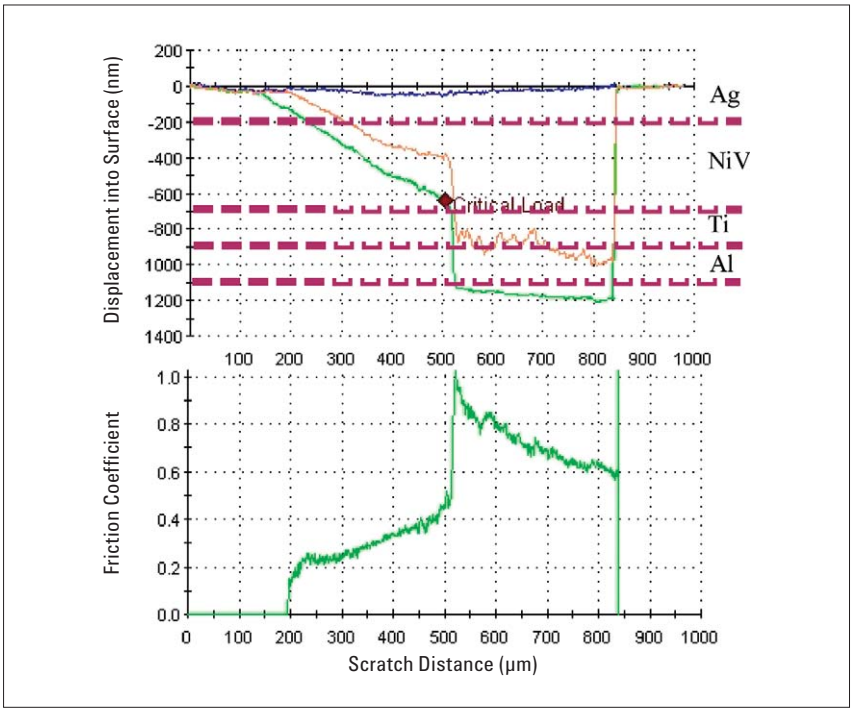

Figure 5. A plot of typical displacement curves and the coefficient of friction versus scratch distance for Sample G4.

versus scratch distance is shown in Figure 4. In Figure 4, the original surface morphology is shown in blue, the actual scratch cycle is shown in green, and the residual deformation is shown in orange. The Critical Load between the film stack and Si substrate was 9.41±0.45 mN, which was 1 mN higher than the Critical Load for the similar samples. All of the tests on this sample smoothly penetrated the Ag layer. Following the smooth transition through the Ag layer, the penetration into the film stopped for a short period of time at the Ag/NiV interface. During this time, the scratch cycle shows further penetration, but this was due to underlying layers deforming as opposed to penetration of the NiV layer. The residual deformation scan confirms that the film penetration stopped briefly between scratch distances of 300 µm and 420 µm. The NiV layer experienced abrupt failure when load reached 6.2±1.3 mN. Three out of five of the tests experienced an abrupt stop to penetration due to the NiV/Ti interface. This interface did not fail smoothly; the residual displacement curve in Figure 4 shows major chipping of the materials around this interface. This chipping continued until the Ti layer was pinned against the Si substrate — typically the soft Al layer would accommodate tremendous plastic deformation prior to failure of the Ti layer and is likely to have completely vacated the region under the scratch test even before the Ti layer failed — and complete failure occurred. An example of the stop in penetration due to the NiV/Ti interface is seen in Figure 4 between the scratch distances of 460 µm and 550 µm; chipping occurred after a scratch distance of 480 µm.

Sample G4

The displacement curves for Sample G4, displayed in Figure 5, show that the Ag layer resists deformation at the start of the test much better than the similar samples (G1 and G9). Consistently, the first 50 µm of the scratch exhibited almost full elastic recovery. The transition between the Ag

and NiV layers was not as consistent as seen in the other samples. While some of the tests had a relatively smooth transition between these first two layers, other tests appeared to blister in the top 200 nm Ag layer. The different transitions were evenly split between the tests: 50% appeared to blister and 50% had smooth transitions. An example of the blistering is shown in Figure 6. Blistering is suspected because the residual displacement curve is jagged in only the upward direction (chipping, which is the alternative to blistering, usually appears as a jagged residual displacement curve that lies above and below the nominal curve). Figure 6 also shows that abrupt failure of the Ag layer occurs at a scratch distance of 420 µm following the blistering of the film; the load at which failure of this layer occurred was 5.41±0.76 mN.

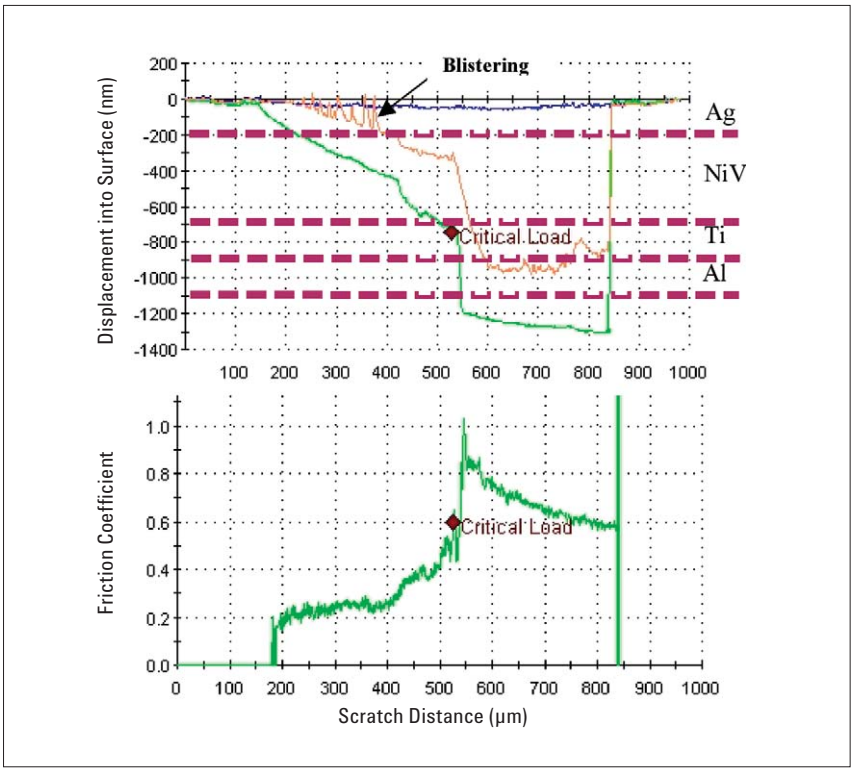

Figure 6. Blistering as seen in the displacement curves for Sample G4.

The transition through the NiV layer was smooth with some minor chipping, but no blistering was apparent in this layer. At a load of 8.49±0.45 mN, the NiV layer abruptly failed. Following the abrupt failure, the Ti layer stopped the transition directly to the substrate, but the Ti and Al layers were gradually chipped off as the test progressed. While Sample G1 always showed complete failure of the films and scratching of the substrate, this sample showed some remaining integrity in the Ti and, possibly, Al layers at the end of the test. Exemplifying the difference in the fracture responses between samples G4 and G1, the coefficient of friction curves for the samples show marked differences following the Critical Loads. Sample G4 shows an increase in the coefficient of friction, but relatively smooth sliding following the failure of the NiV layer. Sample G1, shown in Figure 4, did not show smooth sliding at all and possessed a large variation in the friction following failure of the NiV layer, which is typical of massive chipping.

Sample G9

Figure 7 shows that the scratch tip moves very quickly and smoothly through the Ag layer. It took, on average, 1.21±0.26 mN to penetrate through

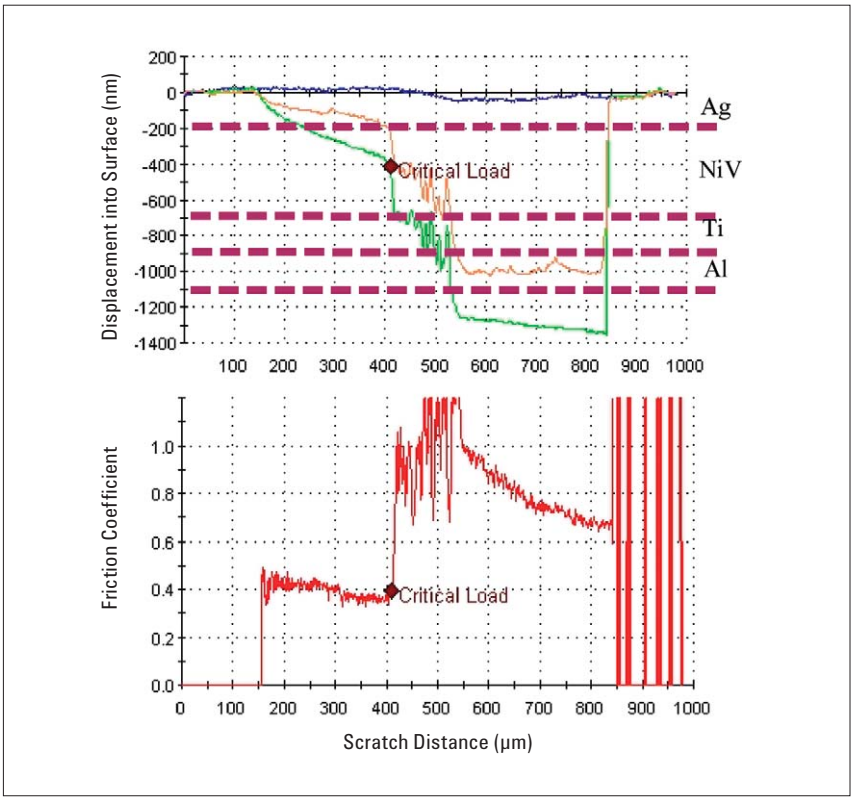

Figure 7. A plot of typical displacement curves and the coefficient of friction versus scratch distance for Sample G9.

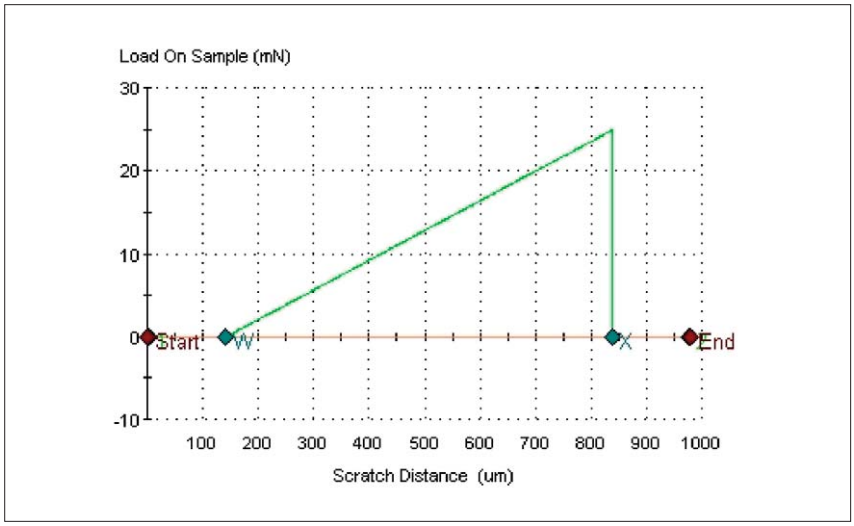

Figure 8. Load on sample versus scratch distance for the ramp-load scratch tests performed on the samples in Group 2.

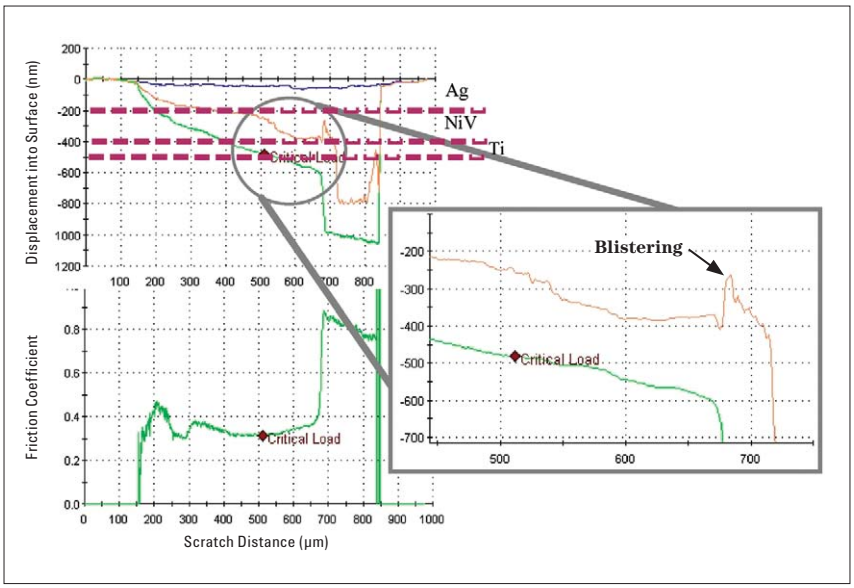

Figure 9. A plot of typical displacement curves and the coefficient of friction versus scratch distance for Sample G2. The outset shows a detailed plot of the failure for the sample.

this layer. An abrupt change in the displacement rate is seen as the scratch tip penetrated the Ag/NiV interface. The scratch tip abruptly penetrated 200 nm into the NiV and the layer abruptly failed at a load of 6.12±1.09 mN. Just as in Sample G1, the NiV/Ti interface did not fail smoothly; the residual displacement curve shows major chipping of the materials around this interface. The test progressed in a similar manner to Sample G1 and massive failure occurred at a load of 8.45±0.5 mN.

GROUP 2

The samples that were tested using ramp-load scratch testing in Group 2 required a higher maximum scratch load to induce consistent failure than did the samples in Group 1. Higher loads were probably required because the Ti layer was applied directly to the Si substrate. The samples in Group 1 had a softer Al layer under the Ti layer, which undoubtedly weakened the Ti layer when scratch loads were applied. A plot of the load on sample versus scratch distance for the tests conducted on Group 2 samples is shown in Figure 8.

Sample G2

A typical scratch test for Sample G2 is shown in Figure 9 along with the coefficient of friction for the scratch cycle. During the scratch test, the tip smoothly penetrated the Ag layer with the penetration rate slowing as the Ag/NiV interface was reached. The interface of the Ag/NiV layer failed abruptly at an average load of 14.2±2.1 mN. Then, the NiV layer was quickly penetrated until the NiV/Ti interface was reached. This interface caused an abrupt stop of penetration for all tests, as seen in the residual deformation curve between scratch distances of 600 µm and 650 µm. The outset in Figure 9 details the failure of the Ti layer. This layer was smoothly scratched until major failure occurred at an average load of 21.0±2.5 mN. All of the tests showed smooth scratching of the Ti layer until blistering of the layer occurred followed by complete film failure. Blistering is typically seen in the residual displacement curve as piled-up material just prior to complete failure.

Sample G3

Typical displacement curves for Sample G3 are displayed in Figure 10. The Ti layer in Sample G3 failed in a similar manner to the Ti layer in Sample G2. However, critical differences are seen in the scratch response of the first interface between the Ag and NiV layers. While the Ag/NiV interface in Sample G2 provided substantial support during the scratch tests, in Sample G3 this interface appeared to be weak and allowed abrupt penetration of the NiV layer immediately down to the Ti layer at a force of 7.7±1.1 mN. Following this abrupt penetration, the Ti layer was chipped away, in some instances very quickly, until massive failure occurred at an average load of 11.45±2.7 mN. The plot of the coefficient of friction in Figure 10 confirms minor chipping of the Ti layer, which appears as a dramatic increase in the coefficient of friction followed by a jagged curve in the coefficient of friction. Notice that in Figure 9 the plot of the coefficient of friction for Sample G2 shows a smooth transition following the Critical Load Marker for failure of the NiV layer until failure of the Ti layer occurred. Similar to the failure of the Ti layer in Sample G2, the Ti layer also blistered in Sample G3 just prior to failure.

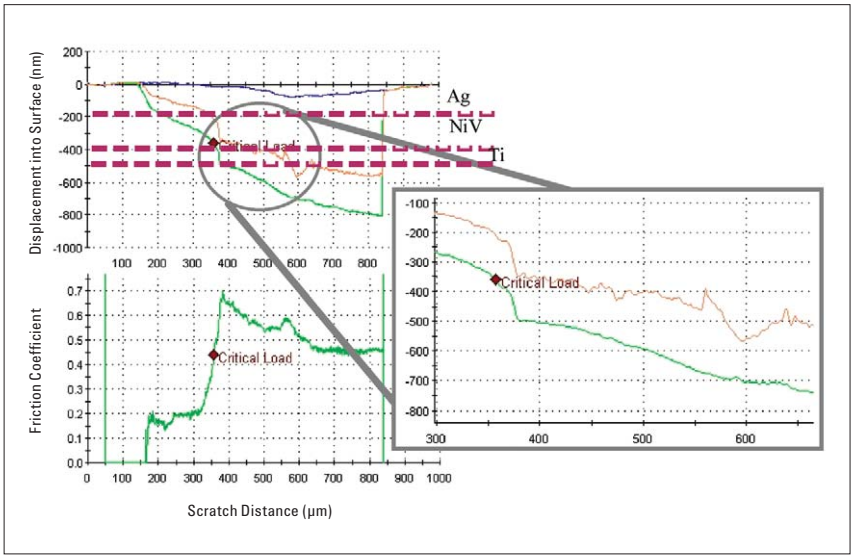

Figure 10. A plot of typical displacement curves and the coefficient of friction versus scratch distance for Sample G3. The outset shows a detailed plot of the failure for the sample.

GROUP 3

Samples G6, G8, and G10 all proved to be the most difficult to characterize due to a peak-to-peak surface roughness of approximately 700 nm. Since the film stack was only 500 nm thick, this made ramp-load scratch tests difficult to interpret; however, new analysis methods showed excellent ability to isolate damage caused by the scratch tests.

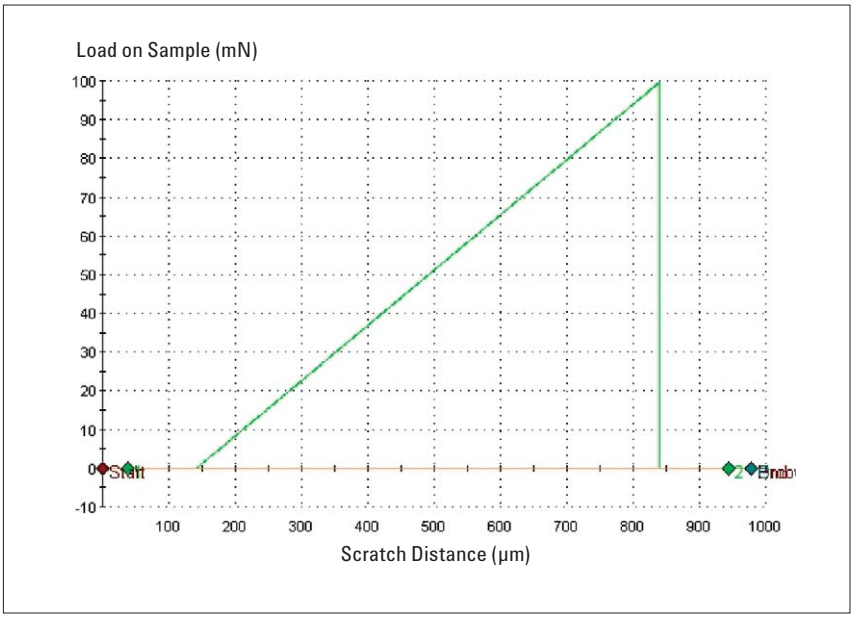

Figure 11. Load on sample versus scratch distance for the ramp-load scratch tests performed on the samples in Group 3.

In order not to shear off asperities on the surface of the sample, a 1 µm radius conical tip was used to perform the scratch tests. This scratch tip also imposed much less stress than the cube-corner tip; therefore, these samples required more load to fracture the film layers. It should be noted that the higher loads used in this group do not imply that the layers are more robust than the other groups; results from tests that have different scratch parameters and tip shapes cannot be compared. A graph of the load on sample versus scratch distance is displayed in Figure 11.

Sample G6

A typical set of displacement curves from testing Sample G6 are shown in Figure 12. The blue trace (the original surface topography) showed that the surface roughness was about 700 nm peak-to-peak. Even though the surface was very rough, differences in the slope of the penetration curves can be seen as the tip penetrates each layer. Since the human eye can be easily fooled into spotting data trends, a new parameter was defined to ensure that the change in penetration was only due to actual film penetration instead of topography change. The "penetration slope" was defined as the rate of change in actual film penetration versus the scratch distance as the tip penetrated into the material. This parameter was calculated by determining the slope of the tip path (i.e., the slope of the displacement curves for both the scratch cycle and the residual deformation scan) and then subtracting the slope of the original surface morphology. This calculation allowed an unbiased examination of the penetration during the scratch with the surface roughness removed from the data. The penetration slope for Sample G6 is graphed in Figure 12 under the displacement curves; the red line on the plot shows the beginning of the actual scratch. The vertical maroon lines divide the test into regions of individual layer response. For example, the scratch tip penetrated the Ag layer and reached the interface between the Ag and NiV layers at a scratch distance of 220 µm. Similarly, the scratch tip penetrated through the NiV layer and reached the interface with the Ti layer at a scratch distance of 405 µm. In the examination of the displacement curves, the benefits of the penetration slope are numerous. Steady penetration of the Ag layer is observed up to 250 µm of scratch distance, followed by slowing as the tip penetration reached the interface with the NiV layer – further penetration is halted, temporarily, at a scratch distance of 310 µm. If not for the graph of penetration slope, it would be easy to conclude that the Ag layer dramatically failed at 210 µm of scratch distance because of the deep step in penetration. However, this step in the displacement curves was actually caused by surface roughness, as seen in the original surface morphology; the penetration slope shows that the tip actually slows in penetration rate as the depth reaches the Ag/NiV interface.

Between the scratch distances of 250 µm and 340 µm, the penetration slope showed initial slowing of penetration as the tip moved past the interface and penetrated the NiV to the second interface with the Ti layer. A brief pause in penetration was seen at a scratch distance of 500 µm, where the penetration slope returned to zero indicating no further penetration. Following the brief pause, the Ti layer completely failed by chipping at an average load of 53.0±1.8 mN.

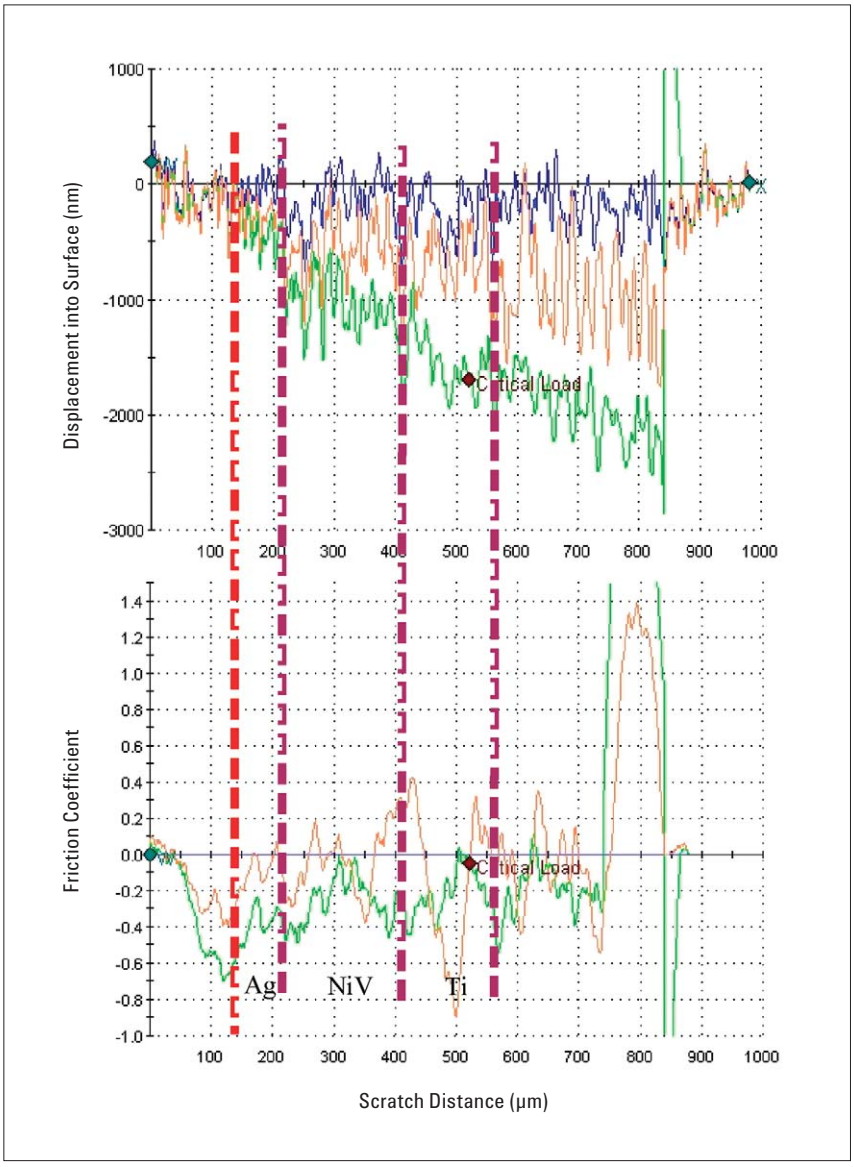

Figure 12. A plot of typical displacement curves and the penetration slope curves versus scratch distance for Sample G6. The red line shows the location of the start for the scratch load application. The vertical maroon lines divide the test into approximate regions of individual layer response.

Sample G8

Sample G8 showed very similar graphical features to those demonstrated in Sample G6. The displacement curves along with the penetration slope curves are displayed in Figure 13 for Sample G8. This graph shows that the Ag layer was penetrated smoothly at a constant rate up to a scratch distance of 280 µm, where the penetration rate abruptly slowed at the Ag/NiV interface. The NiV layer was penetrated at a constant rate up to a scratch distance of 380 µm. At this point, the penetration rate slowed as the tip approached the NiV/Ti interface where the penetration rate dropped back to almost zero. The algorithm for the penetration slope did not do a good job of correcting for the slope of the surface around the scratch distance of 490 µm because the peak-to-peak roughness was almost 1.5 µm; however, the original surface morphology in the displacement curves clearly shows that the unusual anomaly on the surface was the cause of the dramatic change in the penetration slope around this point. The Ti layer failed by either delamination or blistering at an average load of 62.3±5.2 mN; this was almost 10 mN higher than the other two samples in this group.

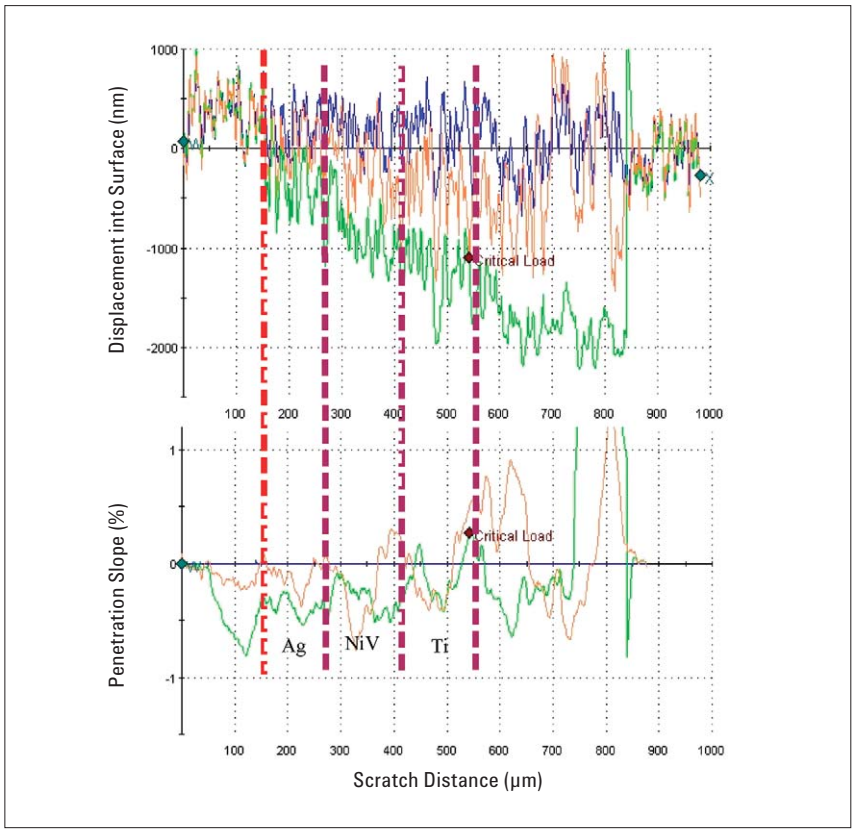

Figure 13. A plot of typical displacement curves and the penetration slope curves versus scratch distance for Sample G8.

Sample G10

The penetration of the Ag layer in Sample G10 quickened as the tip pushed through the top layer until a scratch distance of 210 µm was reached; the displacement curves along with the penetration slope curves for Sample G10 are displayed in Figure 14. Sample G10 experienced an abrupt decrease in the penetration rate at the Ag/NiV interface. The decrease in the penetration rate appears between 210 µm and 250 µm of scratch distance on the penetration slope curves. The slowdown at the interface with the NiV layer was much more abrupt than the other samples tested in Group 3; the dramatic decrease is attributed to the oxide layer in this interface. Notice that at a scratch distance of 120 µm the penetration rate abruptly decreases as compared to samples G6 and G8. The oxide layer between the Ag and NiV appeared to have arrested the penetration for a short period of time until the load reached

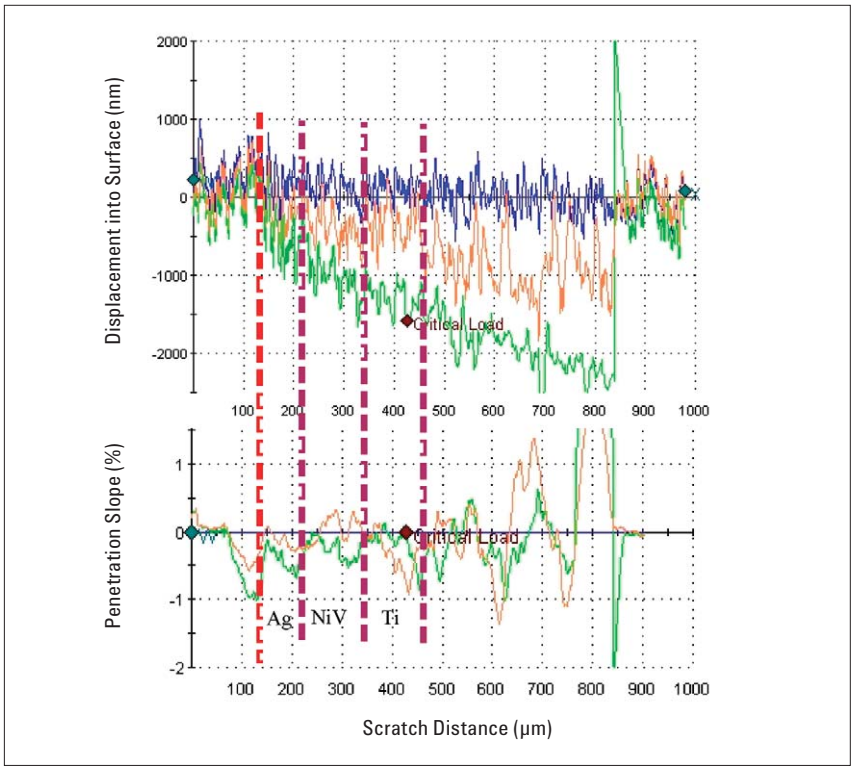

Figure 14. A plot of typical displacement curves and the penetration slope curves versus scratch distance for Sample G10.

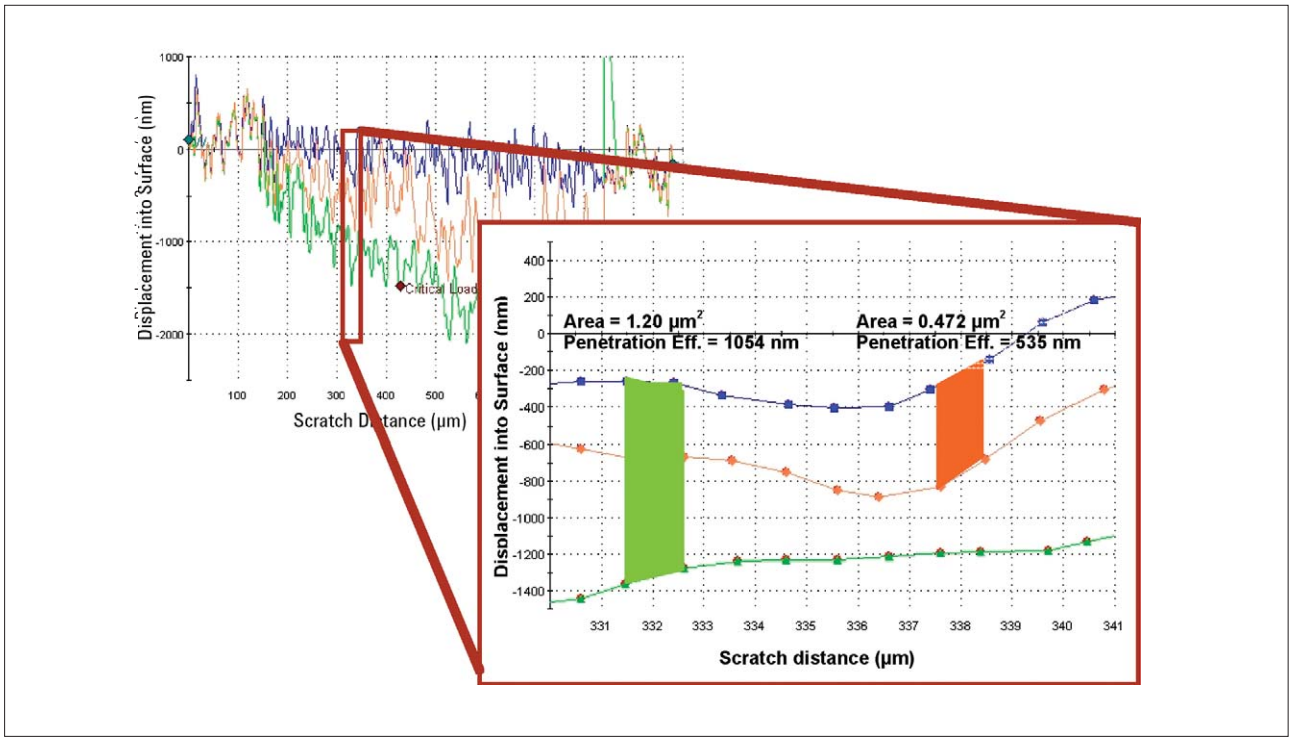

Figure 15. Graphical representation of the calculation for the effective penetration. The green-shaded region is the calculation for the scratch curve, while the orange-shaded region is the calculation for the residual displacement curve.

14.6±0.2 mN. The failure of this layer was easily determined by examining the penetration slope and looking for the location of zero penetration after the initial penetration of the Ag layer; this occurred at a scratch distance of 250 µm in the penetration slope curves of Figure 14. Complete failure of the Ti layer finally occurred at an average load of 42.0±1.37 mN, where chipping of the Ti layer is observed in the residual displacement curve.

Additional Analysis for Rough Surfaces

One additional form of analysis was developed to examine the deformation caused by the scratch tests for the samples with very rough surfaces. This new form of analysis, which ensures that correct analysis of the results was performed, is presented here as an additional tool for analyzing and displaying the results of the scratch tests.

The "effective penetration depth" was developed to calculate the penetration depth based on the area between the displacement curves (i.e., between the scratch curve and the original surface morphology and between the residual deformation curve and the original surface morphology). In performing this calculation, two consecutive data points were used to determine the bounded area of deformation from the displacement curves. Then the area was divided by the change in the scratch distance between the two points. Essentially, the effective penetration depth is the average of the difference between the displacement curves for two consecutive data points. In addition to eliminating the confusion associated with surface roughness, it also has a slight smoothing effect due to averaging. Figure 15 graphically demonstrates the calculation. The green-shaded area is the calculation for the scratch curve, while the orange-shaded region is the calculation for the residual displacement curve. For a comparison, the plots shown for Group 3 (Figures 12 through 14) were

transformed into effective penetration plots in Figure 16. The major advantage of these plots is that they show film penetration as opposed to a combined measurement of film penetration and surface roughness. The deformation and failure revealed by these plots support the prior failure analysis.

Conclusions

Several multilayered thin metallic films were tested using the Agilent Nano Indenter G200. The observation of the displacement curves and the coefficient of friction during the tests showed clear differences in the scratch response of individual layers in the samples, as well as clear differences among the samples themselves. The three groups of samples highlighted the need for flexible test protocols and methods in producing measurable failure. Each sample group posed different challenges, whether testing very rough surfaces for failure or measuring Critical Loads between inner layers. Table 3 shows the summary of results for the three groups of samples from the ramp-load scratch tests.

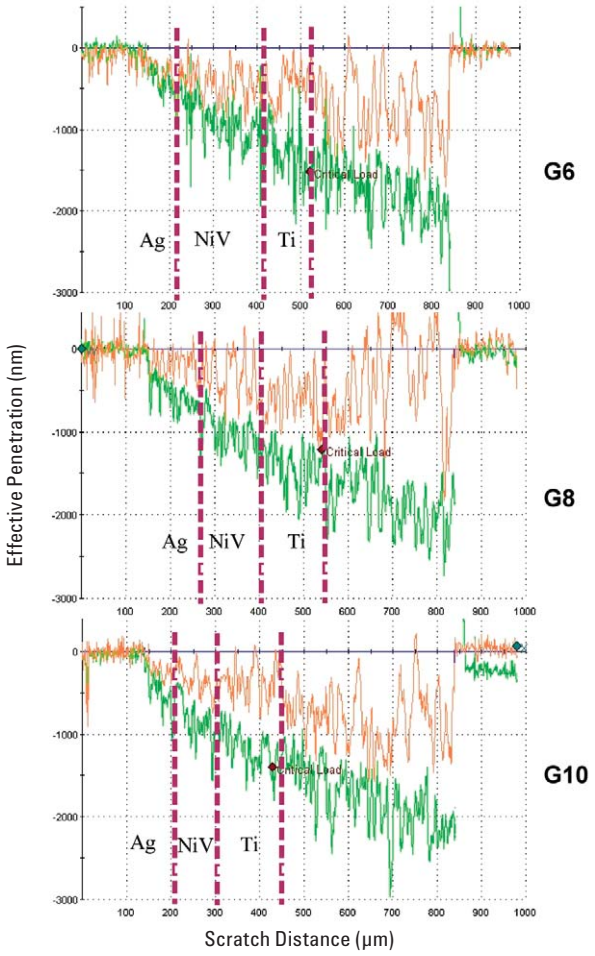

Figure 16. Effective penetration graphs for the three samples in Group 3. These graphs can be compared directly to figures 12 through 14, respectively. The blue traces along the x-axis show the original surface morphology, which is now just a straight line in these plots.

Group	Sample	Layer	Critical Load (mN)	Failure Type
1	G1 – Good	NiV	6.21±1.32	Delamination
		Ti	9.41±0.45	Chipping
		Stack/Si	9.41±0.45	
	G4 – Bad	Ag	5.41±0.76	Plastic Deformation/Blistering
		NiV	NA	Plastic Deformation
		Ti	8.49±0.45	Delamination/Chipping
		Stack/Si	8.49±0.45	
	G9 – Bad	Ag	1.21±0.26	Plastic Deformation/Delamination
		NiV	6.12±1.09	Chipping/Plastic Deformation
		Ti	8.45±0.51	Chipping
		Stack/Si	8.45±0.51	
2	G2 – Good	NiV	14.2±2.1	Delamination/Chipping
		Ti	21.0±2.5	Blistering
	G3 – Bad	NiV	7.7±1.1	Delamination
		Ti	11.45±2.7	Chipping & Blistering
3	G8 – Good	Stack/Si	62.3±5.2	Delamination/Blistering
	G6 – Bad	Stack/Si	53.0±1.8	Chipping
	G10 – Bad	Ag/NiV interface	14.6±0.2	Delamination/Chipping
		Stack/Si	42.0±1.37	Chipping

Table 3. Summary of scratch results for the three groups of samples. Layers that only displayed plastic deformation and no fracture are not listed.

Scratch testing on Group 1 samples provided an excellent technique for differentiating the samples. All of the samples showed slightly different scratch responses for each layer and the layers showed different types of failures. It was clear that Sample G1, the "good" sample, had a higher critical load than the other samples, which was predominately due to its Ti layer.

The samples in Group 2 required much more load to fracture the Ti layer than samples in Group 1; this was most likely because the Ti layer was deposited directly on the Si substrate, which is much harder than layers of Al. The most notable difference in these samples was the performance of the NiV layer: Sample G2 supported twice the load as compared to Sample G3 for this layer. In addition, the Ti layer in Sample G2 scratched smoothly until the layer blistered and delaminated from the substrate, while Sample G3 chipped during the scratching of the Ti layer and then experienced blistering and complete failure.

Rough films are usually very difficult to characterize; however, two newly developed analysis techniques designed to remove the majority of the influence of surface topography in the results had a major impact in the successful analysis of film failure for samples in Group 3. The "penetration slope" provided a measure of the rate at which each layer was penetrated and clearly showed layers that provided excellent resistance to penetration. In addition, the "effective penetration depth" used the area bounded by the displacement curves to determine the effective penetration; this parameter removed the influence of the surface roughness and marginally smoothed the displacement curves. For these samples, the oxide layer between the Ag and the NiV layer, along with the adhesion quality of the Ti layer, were the primary differentiators.

Many techniques were evaluated to determine the optimal test methods and parameters for analyzing each group of samples. The samples with smooth surfaces tested very well when using a cube-corner tip in the face-forward direction. The Lateral Force Measurement (LFM) option was helpful in determining and verifying the type of failure that occurred in each layer for these smooth samples. This is in stark contrast to the rough samples. The LFM contained too much noise to be of any use in evaluating fracture of the rough samples. It is suspected that a larger radius tip would have made the LFM more useful on the samples with rough surfaces. In addition, the cube-corner tip was much too aggressive for the samples with high surface roughness. A conical tip with a larger tip radius than the cube-corner tip was used when testing these samples so that surface asperities were rolled over as opposed to sheared.

Nano Mechanical Systems from Agilent Technologies

Agilent Technologies, the premier measurement company, offers high-precision, modular nano-measurement solutions for research, industry, and education. Exceptional worldwide support is provided by experienced application scientists and technical service personnel. Agilent's leading-edge R&D laboratories ensure the continued, timely introduction and optimization of innovative, easy-to-use nanomechanical system technologies.

www.agilent.com/find/nanoindenter

Americas

Canada	(877) 894 4414
Latin America	305 269 7500
United States	(800) 829 4444

Asia Pacific

Australia	1 800 629 485
China	800 810 0189
Hong Kong	800 938 693
India	1 800 112 929
Japan	0120 (421) 345
Korea	080 769 0800
Malaysia	1 800 888 848
Singapore	1 800 375 8100
Taiwan	0800 047 866
Thailand	1 800 226 008

Europe & Middle East

Austria	43 (0) 1 360 277 1571
Belgium	32 (0) 2 404 93 40
Denmark	45 70 13 15 15
Finland	358 (0) 10 855 2100
France	0825 010 700*
	*0.125 €/minute
Germany	49 (0) 7031 464 6333
Ireland	1890 924 204
Israel	972-3-9288-504/544
Italy	39 02 92 60 8484
Netherlands	31 (0) 20 547 2111
Spain	34 (91) 631 3300
Sweden	0200-88 22 55
Switzerland	0800 80 53 53
United Kingdom	44 (0) 118 9276201

Other European Countries:
www.agilent.com/find/contactus

Printed in USA, April 7, 2010
5990-5701EN

Agilent Technologies